



Capabilities of optical and radar Earth observation data for up-scaling methane emissions linked to subsidence and permafrost degradation in sub-Arctic peatlands

Sofie Sjögersten¹, Martha Ledger¹, Matthias Siewert², Betsabé de la Barreda-Bautista^{1,3}, Andrew Sowter⁴, David Gee⁴, Giles
5 Foody³, Doreen S. Boyd³

¹University of Nottingham, School of Biosciences, College Road, Sutton Bonington, Loughborough, LE12 5RD, UK

²University of Umeå, Department of Ecology and Environmental Sciences, KB H4, Linnaeus väg 6, Umeå universitet, 901
87 Umeå, Sweden

10 ³School of Geography, University of Nottingham, University Park, Nottingham, NG7 2RD, UK

⁴Terra Motion Ltd, Ingenuity Centre, Triumph Rd, Nottingham NG7 2TU, UK

Correspondence to: Sofie.Sjogersten@nottingham.ac.uk

Abstract. Permafrost thaw in Arctic regions is increasing methane (CH₄) emissions to the atmosphere but quantification of such emissions is difficult given the large and remote areas impacted. Hence, Earth Observation (EO) data are critical for
15 assessing both permafrost thaw, associated ecosystem change, and increased CH₄ emissions. Often extrapolation from field measurements using EO is the approach employed. However, there are key challenges to consider - that landscape CH₄ emissions result from a complex local-scale mixture of micro-topographies and vegetation types that support widely differing CH₄ emissions and the difficulty in detecting the initial stages of permafrost degradation before vegetation transitions have occurred. This study considers the use of a combination of ultra-high resolution unoccupied aerial vehicle
20 (UAV) data, together with Sentinel-1 and -2 data to extrapolate field measurements of CH₄ emissions from a set of vegetation types which capture the local variation in vegetation on degrading palsa wetlands. We show that the ultra-high resolution UAV data can map spatial variation in vegetation relevant to variation in CH₄ emissions and extrapolate these across the wider landscape. We further show how Sentinel-1 and Sentinel-2 can be used. By way of a soft classification, and simple correction of misclassification bias of a hard classification, the output vegetation mapping and subsequent
25 extrapolation of CH₄ emissions matched closely that generated using the UAV data. InSAR assessment of subsidence together with the vegetation classification suggested that high subsidence rates of palsa wetland can be used to quantify areas at risk of increased CH₄ emissions. We estimate that a transition of an area currently experiencing subsidence to fen type vegetation are estimated to increase emissions from 116 kg CH₄ season⁻¹ from the 50 ha study area, to emissions as high as 6500 to 13000 kg CH₄ season⁻¹. The key outcome from this study is that a fusion of EO data types provides the ability to
30 estimate CH₄ emissions from large geographies covered by a fine mixture of vegetation types and vulnerable to transitioning



to CH₄ emitters in the near future. This points to an opportunity to measure and monitor CH₄ from the Arctic over space and time with confidence.

1 Introduction

35

The severe impact of climate heating in the Arctic has raised grave concerns of positive feedbacks from ecosystems that store substantial amounts of soil organic carbon in soils and peat deposits (Hugelius et al., 2020; Mishra et al., 2021; Sjöberg et al., 2020; Schneider Von Deimling et al., 2012; Chadburn et al., 2017; Grosse et al., 2016; Biskaborn et al., 2019). Although the overall carbon balance in permafrost and non-permafrost peatlands is similar (Olefeldt et al., 2012), permafrost
40 thaw increases methane (CH₄) emissions across a range of Arctic landscapes (Olefeldt et al., 2013). Any increase in emissions of CH₄ is of particular concern, as it is a powerful greenhouse gas in a global context, with Arctic ecosystems acting as strong emitters of CH₄ (Mcguire et al., 2009; Turetsky et al., 2020; Euskirchen et al., 2014; Maksyutov et al., 2010; Glagolev et al., 2011).

Palsa are elevated peat mounds with a frozen core formed in peatlands and are a common landform in the sporadic
45 and discontinuous zone of the permafrost region where palsa peatlands cover ca. 20% of the total permafrost region (Ballantyne C. K., 2018; Tarnocai et al., 2009). From a climate feedback perspective, these are critical systems as they are carbon (C) rich, with an estimated storage of 100 Gt C (based on data in (Tarnocai et al., 2009; Schuur and Abbott, 2011). Palsa peatland are dynamic systems that comprise of raised peatland plateaux, which can vary in size from tens of meters to kilometers in size, these plateaux are often surrounded by lower lying waterlogged areas or have borders with thermokarst
50 lakes (Ballantyne C. K., 2018; Zuidhoff and Kolstrup, 2000). As a result of the raised nature of palsa their surface tend to be relatively dry. However, this changes as the permafrost in these peatlands degrade and the peat surface subsides which, over time, results in waterlogging (Sjöberg et al., 2015; Olvmo et al., 2020). Such degradation is already being observed in many areas of the Arctic in response to the greater than average warming occurring in this region (Åkerman and Johansson, 2008; Sannel et al., 2016; Olvmo et al., 2020; De La Barrera-Bautista et al., 2022; Borge et al., 2017; Luoto and Seppälä, 2003;
55 Sannel and Kuhry, 2011). The loss of permafrost and switch to waterlogged conditions represents a profound change in how this ecosystem functions, driving increased CH₄ emissions which has been observed across many Arctic landscapes (Miglovets et al., 2021; Varner et al., 2022; Glagolev et al., 2011; Walter Anthony et al., 2016; Walter et al., 2006). To understand fully the magnitude of these feedbacks and their impacts on the global climate, it is imperative to both quantify current emissions and predict new areas that may become CH₄ emitters across Arctic landscapes undergoing permafrost
60 degradation.

Given the size of the areas under threat from warming and their remoteness, remote sensing techniques are necessary to detect when and where permafrost degradation and subsidence is occurring. Coupled with measures of CH₄ flux, this may offer an approach for understanding, estimating, and predicting CH₄ feedbacks at landscape scales across permafrost peatlands of the circumarctic region. Detecting year-to-year degradation of permafrost manifested as subsidence



65 is possible using the Advanced Pixel System using Intermittent Baseline Subset (ASPIS-InSAR) and other InSAR
techniques (Sowter et al., 2016; Gee et al., 2017; Cigna and Sowter, 2017; Alshammari et al., 2020; Alshammari et al., 2018;
Bradley et al., 2021; De La Barreda-Bautista et al., 2022; Van Huissteden et al., 2021). Measures of surface subsidence of
permafrost affected areas and the rate of ground motion can give an indication of permafrost degradation extents and rates.
Furthermore, the ASPIS-InSAR data is unaffected by clouds, is based on freely available Sentinel-1 data, and can be used to
70 analyse impact at continental scale. This means that ASPIS-InSAR can be used to identify areas that are at risk of increased
CH₄ emissions and help to assess the radiative forcing ecosystem feedback resulting from permafrost thaw.

Complimentary remote sensing derived vegetation maps can be used to extrapolate plot based CH₄ emission data to
the wider landscape (Varner et al., 2022). However, the scale-dependency of ecosystem properties that are non-linearly
distributed in space (Siewert, 2018; Siewert and Olofsson, 2020) means that the spatial resolution of the remotely sensed
75 data are important. Coarse spatial resolution remote sensing data, such as that from openly available and high temporal
optical satellite-borne sensors, run the risk of missing small areas of those vegetation types with high CH₄ emissions, which
may lead to an underestimate of total emissions. Further, the relatively slow rate of the response of vegetation to ground
condition changes resulting from permafrost degradation means mapping vegetation may not fully explain patterns of CH₄
emissions. After subsidence starts to occur, the original vegetation type can persist for many years (>10 years) until the site
80 conditions have changed to a point that the original vegetation is outcompeted (Johansson et al., 2013). This makes it
difficult to use vegetation change in isolation as a year-on-year proxy for permafrost degradation and linked potential
regulation of CH₄ emissions. Furthermore, permafrost degradation and linked increases in CH₄ production, is driven by
several processes across scales. Variation in root inputs of labile carbon or oxygen in the peat profile occur over millimeters
and can vary seasonally in response to water levels. Lateral erosion and subsidence linked to permafrost degradation occur
85 on meter scales when measured over several years, while changes in the vegetation community from raised palsa vegetation
to fen type vegetation occur over tens of meters at decadal time-scales. Together the different processes associated with
permafrost degradation result in a spatially varied landscape with a mixture of functionally distinct geomorphological units
with regard to soil moisture content and vegetation productivity, creating a palimpsest of processes and properties
determining the effective greenhouse gas feedback of these regions (Siewert et al., 2021). Therefore, remote sensing
90 methodologies which capture fine-scale spatial variation in vegetation composition, in addition to permafrost degradation
over seasonal to yearly time scales, are needed to provide appropriate observations of degrading peatlands in the Arctic in
order to measure their CH₄ emissions accurately.

With a view to estimating CH₄ emissions resulting from permafrost degradation in peatlands, this paper explores
two remote sensing technologies to provide data for extrapolating plot-based methane measurements over sub-Arctic
95 peatlands of northern Sweden. Specific objectives were to (i) carry out detailed field surveys to capture small-sized or local-
scale variation in CH₄ emissions linked to vegetation type and permafrost subsidence; (ii) conduct vegetation mapping from
Sentinel-2 satellite data, and in particular demonstrate the value of rigorous map validation on the quantification of CH₄



emissions; and (iii) quantify CH₄ emissions from areas experiencing permafrost degradation and those at high risk of subsidence as determined from Sentinel-1 InSAR (processed using ASPIS) data.

100

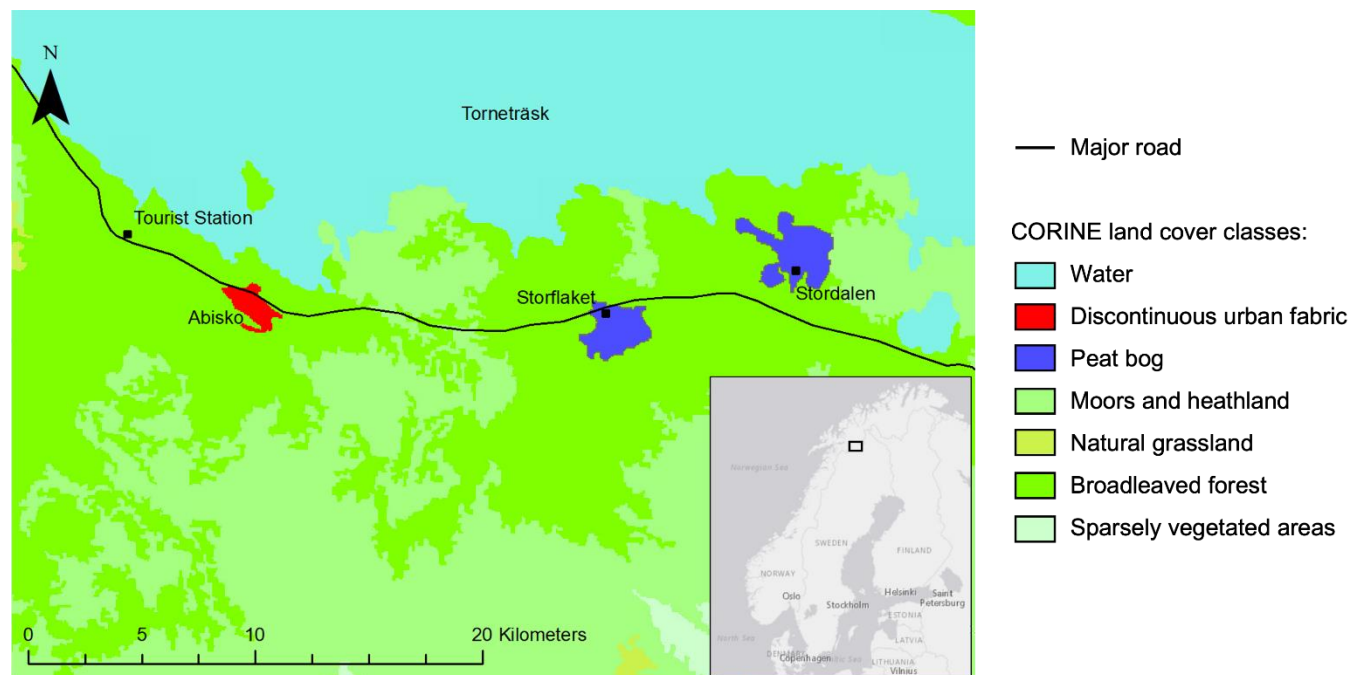
2 Methods

2.1 Field site description

Three peatland locations affected by permafrost conditions - the Tourist Station, Storflaket, and Stordalen wetlands (Figure 1) - situated to the south of Lake Torneträsk near Abisko, northern Sweden (68°12'N, 19°03' E, 351 masl), were the focus of study. The study sites are in sub-Arctic climatic zone, the mean annual temperature (MAT) ranges between 0.8 and 1.0 °C and the mean annual precipitation (MAP) ranges from 304 and 424 mm, in the West and in the East, respectively. The study sites comprise areas of raised palsas (i.e. relatively dry peat plateaus) and waterlogged areas with fen or birch forest vegetation. All three sites show signs of active permafrost thaw indicated by a lowering of the ground surface (i.e. ground subsidence), high soil moisture levels, and areas of palsa collapse (i.e. complete permafrost degradation and transition from palsa to wetland) (Åkerman and Johansson, 2008).

Previous mapping of the vegetation at these sites using Unoccupied Aerial Vehicles (UAVs) and subsidence estimated using ASPIS-InSAR (De La Barreda-Bautista et al., 2022) show the vegetation on the palsa to be composed of bryophytes (e.g. *Sphagnum fuscum*), lichens and dwarf shrubs (*Empetrum nigrum*, *Andromeda polyfolia*, and *Betula nana* (Sjögersten et al., 2016)). The most common herbaceous species was *Rubus chamaemorus*. Recently collapsed areas adjacent to and within the plateau areas tended to be vegetated by *Sphagnum* sp. and *Eriophorum vaginatum* and *E. angustifolium*. Extensively collapsed and subsequently flooded areas tended to be vegetated by graminoids, mainly *Carex* and *Eriophorum* species, herbaceous plants mainly *Menyanthes trifoliata*, *Comarum palustre*, and deciduous shrubs, such as *Salix lapponica*, *Salix ssp.* and *Betula nana*. Forested wetland areas tended to be located adjacent to streams and at the perimeters of the wetland areas. The mean peat depth was ca 60, 94, 50, and 40 cm, on palsas, *Sphagnum* sp., sedge, and forested wetland areas, respectively; mean soil C storage in the top 100 cm was 52, 34, 33, 40 kg SOC m⁻² for palsa, *Sphagnum* sp., sedge, and forested wetland, respectively (Siewert, 2018). The depth of the active layer (the seasonally thawed upper part of the soil) varies between drier areas, which have a shallower (ca 30 – 60 cm) active layer, and wetter areas, where the active layer is deeper or where there is no permafrost at all in the upper 1.5 m. In the Torneträsk area, the active layer depths have increased, between 0.2 and 2.0 cm yr⁻¹ over 1978-2006, with a higher rate in more recent years (Åkerman and Johansson, 2008).

125



130 **Figure 1. Map showing the location of the three permafrost peatland study sites: Tourist Station, Storflaket and Stordalen. Inset: Location of Abisko in northern Sweden. The landcover classes were based on the CORINE land cover classification.**

2.2 Experimental design

135 The fieldwork to measure CH₄ emissions at the three study sites was carried out across the dates of 8-15 June, 18-29 of July and 8-12 of September 2021. At each site, we targeted six common vegetation types, dry lichen, dwarf shrub, moist moss, sphagnum wetland, sedge wetland and willow wetland. We also measured CH₄ emissions from subsiding areas with dry lichen, dwarf shrub and moist moss vegetation types. Measurements in each vegetation type were carried out in blocks of ca 10 m diameter with 3-5 sampling points in each block. Sampling blocks were distributed across the sites and for the majority of vegetation types data from at least two spatially separate (i.e. > 100 m apart) blocks were collected. As the dry lichen subsiding vegetation type was not common, this vegetation was sampled less than the other classes. To facilitate the collection of spatially distributed data from the common vegetation types, we selected sites with relatively easy access (e.g. sampling of water logged areas were made in parts of the sites accessible by boardwalks). This approach allowed us to collect CH₄ flux data from a large number of sampling points with the aim to generate scalable data from each vegetation type. A total number of 502 measurements were collected across the three sites and the three dates, with all vegetation types measured in several locations at each site. Specifically, on the raised palsas and subsiding palsa areas, the total number of measurements point were 47 and 9 for dry lichen (DL) and dry lichen subsiding (DLS), respectively, 42 and 68 for dwarf shrub (DS) and dwarf shrub subsiding (DSS), respectively, 50 and 56 moist moss (MM) and moist moss subsiding (MMS),



150 respectively. In the flooded fen vegetation areas, 102, 78 and 50 measurement points were in *Sphagnum* wetland, sedge wetland and willow wetland, respectively. Detailed description of the vegetation types are in de la Barreda Bautista et al. (2022). Additional measurements of soil temperature and moisture using a Theta probe connected to a Theta meter (Delta-T devices, Cambridge, UK) were carried out in each point where methane emissions were measured. The active layer depth was determined using a graded metal pole in a subset of plots (ca 10 of each vegetation type in each of the three mires in June, July and Sept 2021 (De La Barreda-Bautista et al., 2022).

155 2.3 CH₄ emissions measurements

Methane flux measurements were conducted using a dynamic closed chamber connected to a Los Gatos ultraportable GHG analyser (San Jose, California, USA). Two types of chambers were used, one 15 and one 40 cm tall, the diameter was 40 cm. The chambers were equipped with two push-fit connectors that acted as an inlet and outlet allowing the gas to flow from the chamber to the analyser and then to flow back into the chamber. After the chamber was placed on the measuring point, it was gently pushed on a 5 cm deep groove in the peat to create an airtight headspace between the ground surface and the chamber walls. To reduce problems with bubbles being released into the chamber the chamber was first placed on the ground and then lifted and allowed to vent. The chambers were then placed back on the ground and the sampling tubes connected. The soil CH₄ concentration (in ppm) increment inside the chamber was measured during 4 to 6 minutes, with data automatically recorded every 20 seconds. If the change in CH₄ concentrations was not linear, the measurement was stopped, chambers lifted from the soil and a new measurement was taken after CH₄ readings had stabilized.

Trace gas concentrations, determined by the Los Gatos instrument, were converted to mass units using the ideal gas law (Eq. 1). Thereafter, using of the slope of the linear change in gas concentration over time and Eq. 2, CH₄ fluxes were calculated. Positive fluxes indicated GHG emissions from the soil into the atmosphere and negative fluxes indicated and uptake of atmospheric GHG by the soil.

170

$$n = \frac{PV}{RT} \quad (1)$$

$$F = \frac{\text{Slope} \times \text{Volume}_{\text{chamber}}}{\text{Area}_{\text{chamber}}} \quad (2)$$

175 where, n is the number moles of trace gas (mol L^{-1}), P is the atmospheric pressure (Pa), V is volume of trace gas per litre of air (L L^{-1}), R is the gas law constant ($8314.46 \text{ L} \cdot \text{Pa} \cdot \text{K}^{-1} \cdot \text{mol}^{-1}$), and T is the temperature (K). F is the calculated flux for either CH₄ or N₂O ($\text{mol m}^{-2} \text{ hr}^{-1}$), Slope is the slope of the linear regression ($\text{mol L}^{-1} \text{ hr}^{-1}$), $\text{Volume}_{\text{chamber}}$ is chamber headspace volume (L) and $\text{Area}_{\text{chamber}}$ is the area of the chamber (m^2). Fluxes were converted to $\mu\text{g m}^{-2} \text{ h}^{-1}$ using the molecular weight of CH₄ (i.e. 16.04 g mol^{-1} , respectively). To avoid excluding very small CH₄ fluxes from the annual calculations, fluxes with low r^2 were used in the calculation of cumulative emissions. By contrast, large CH₄ fluxes with low

180



r^2 were discarded as these fluxes were considered to be either affected by CH₄ ebullition, gas leakage or gas under pressured during transportation of vials. Seasonal fluxes were calculated to the thaw period (i.e. spring-autumn) by scaling the CH₄ flux measurements made in June, July and September to the length of the spring season, summer season and autumn periods, respectively, and then summing these. The length of the three seasons was determined using a combination of seasonal
185 NDVI data from the Torneträsk valley station (Siewert and Olofsson, 2020) and long term air temperature data from Abisko (www.smhi.se).

2.4 UAV-captured data for Digital Elevation Models (DEMs) and vegetation mapping

Multispectral and true colour RGB data ultra high resolution (UHR) data were captured across Storflaket and Stordalen in
190 2020 and from the Tourist St. site in 2021 from ca 106 and 100 m height using a fixed-wing UAV - Sensefly Ebee fitted with a Parrot Sequoia multispectral sensor. The Parrot Sequoia obtained spectral measurements across four bands: Green (550nm ± 40nm), Red (660nm ± 40nm), Red Edge (735nm ± 10nm) and Near Infrared (790nm ± 40nm). The images were processed using Pix4D (Berlin, Germany) to produce an orthomosaic for each spectral band. This resulted in a ground resolution of ~11-13 cm for the multispectral and 2-3 cm for the RGB data. To ensure the orthomosaic and DEM were accurately
195 geolocated we collected ca 50 ground control points using a differential GPS (dGPS; Trimble R8s) across all three sites. Further details on the UAV data collection are in de la Barreda Bautista et al. (2022).

The multispectral UAV data was resampled to 0.5m spatial resolution and then classified to produce a vegetation type map for the three study sites using the same nine classes (i.e. the dominant vegetation types found on raised palsa plateaux's, dry lichen, dwarf shrub and moist moss vegetation and areas covered by those vegetation types impacted by
200 subsidence, plus three vegetation types which dominate the flooded areas: *Sphagnum* moss, sedge and willow wetland) as those for which *in situ* CH₄ flux data were measured. A Support Vector Machine classification approach (Foody and Mathur, 2004) was used in ArcMap 10.4 (ESRI) using the Train Support Vector Machine Classifier in the Spatial Analyst package, with simple random sampling of ground data in June 2021 for Storflaket ($n = 258$) and Stordalen ($n = 395$) sites and August 2021 for the Tourist Station ($n = 657$). The ground points from each site were randomly split into training and validation
205 datasets of 70% and 30% proportions.

2.5 Sentinel-2 remotely sensed data for vegetation mapping

We used a neural network classification approach (Xie et al., 2008) within QGIS desktop 3.16.5. to predict vegetation cover over the three sites of interest using Sentinel-2 data (wavebands 2, 3, 4, 5, 6, 7, 8a, 11 and 12) and elevation, slope and
210 roughness data derived from the ArcticDEM, optical-stereo imagery model at 2 m spatial resolution (Morin et al., 2016). To match the 20 m × 20 m resolution of the Sentinel-2 pixels, an average elevation was computed for each pixel. Sentinel-2 wavebands 2, 3 and 4 were re-sampled from 10 m to 20 m resolution using nearest neighbour interpolation to match the resolution of the other wavebands. The UAV-derived vegetation maps were used to train the Sentinel-2 scenes covering the three study sites of the Tourist Station, Storflaket and Stordalen - for this the UAV data was upscaled to 20 m × 20 m using



215 majority classification, this yielded a dataset of 2376 pixels. Training and test datasets were created from this. The testing set
used was generated as a random stratified sample comprising 50 pixels per vegetation class, unless there was less than that
(e.g., the willow wetland class had only 20 test pixels).

The neural network approach was used to classify the Sentinel-2 data into vegetation classes from which the total
areal extents of each vegetation class across the three sites were calculated. Specifically, a multi-layer perceptron network
220 with backpropagation and weight backtracking was used, therefore the ‘learning rate’ and ‘momentum’ parameters were not
required (Xie et al., 2008). Two neural networks were generated: one that produced a standard hard classification (i.e., a
single class label is produced for each pixel) and one that produced a soft classification (i.e., grades of class membership is
produced for each pixel). The optimal model structure for the majority and the soft classification approaches consisted of
225 twelve principal components, normalised between 0-1, one hidden layer with three neurons (hard classification model) or ten
neurons (soft classification model) and an output layer of fifteen units corresponding to the land cover types identified within
the three study sites. Both models were developed through trial and error and iteration to arrive at the maximum overall
accuracy. The soft classification was undertaken as it enables the estimation of the proportion of different vegetation types
within each pixel offering greater understanding of the area covered by each class, in particular to capture and map those
smaller patches of vegetation that have a larger contribution to CH₄ flux.

230 Misclassification errors in the maps may substantially bias estimates of class areal extent generated from the maps.
An adjustment for misclassification bias in a map can be made if its accuracy has been rigorously evaluated. Here, good
practice methods for accuracy and area estimation (Olofsson et al., 2013; Olofsson et al., 2014) were followed to produce
misclassification bias adjusted estimated of class area; an adjustment for the soft classification would ideally require more
detailed ground reference data than was available. Thus in total, three vegetation type outputs (maps and class areal extents)
235 from the Sentinel-2 data were produced (soft classification; hard classification and misclassification bias hard classification).
The areal estimates of the vegetation classes were subsequently multiplied with the mean CH₄ fluxes measured for each
vegetation class to produce CH₄ budgets for the entire mapped area.

240 **2.6 Surface motion from Sentinel-1 InSAR**

We used C-band SAR data from the Sentinel-1 satellites (European Union’s Copernicus Programme) to map multi-annual
average velocity, subsequently denoted surface motion of the study areas. Details of this approach are in de la Barreda
Bautista et al, 2022. Briefly we gathered images from 2017 to 2020, focusing on the thaw season between April and October
for three separate years. A total of 125 images were acquired from the descending mode and surface motion was obtained
245 using the APSIS method (formerly known as ISBAS), which relaxes the requirement for consistent phase stability for all
observations using a coherence threshold of 0.45. Following InSAR processing the ground resolution was 20 m x 20 m.
Using a stable reference point located in the centre of Abisko village first the multi-annual average velocity (or average
surface displacement) between 2017 and 2020 (with negative values representing subsidence) was calculated and second, for



each season, a time series of surface motion was produced, showing the change in relative height of the surface. Surface
250 motion range for the 2017 and 2020 thaw periods were calculated by subtracting the minimum surface motion value from the
maximum surface motion value within respective time series between June and October. The InSAR data were thereafter
compared to the CH₄ flux data as described in the statistical analysis section below.

2.7 Statistical analysis

255 We used residual maximum likelihood (REML) mixed models to test for significant differences in CH₄ fluxes among sites
and vegetation and their interactions. For this analysis we used vegetation type as the fixed effect and sampling location (i.e.
block), month and site as random effects. The residuals were inspected to ensure the normality assumption of the analysis
was met. The standard error of the difference was used to evaluate which vegetation types that differed from each other. We
tested for the relationships between the UAV predicted CH₄ budgets per vegetation type and the three different Sentinel-2
260 based classifications using linear regression analysis. Relationships between ASPIS-InSAR linear motion between the 2017
and 2020 thaw periods and seasonal CH₄ fluxes were explored using REML in which the ground motion categorised into 2.5
mm ranges were used as the fixed effects and site as the random effect. For this analysis comparison, the CH₄ fluxes
extrapolated for each target vegetation type to the three sites using the VHR UAV data, which are able to capture the local-
scale variation in the vegetation types, were aggregated to the 20×20 m pixel size of the InSAR data.

265

3 Results

3.1 Variation in CH₄ fluxes linked to vegetation type and permafrost degradation

270 The intact raised tundra vegetation types (DL, DS and MM) had generally low CH₄ fluxes; the dry lichen vegetation type even
acted as a weak CH₄ sink in spring (Figure 2a). The areas identified as showing signs of permafrost degradation/subsidence
had higher soil moisture content ($F_{8,489} = 167.91$, $P < 0.001$; $SED = 3.6\%$; Figure 3a) and deeper active layer depths ($F_{7,163} = 27$
 $P < 0.001$ and $F_{8,91} = 8.15$, $P < 0.001$, for July and September, respectively; Figure 4) than areas that were less affected by
degradation. Degrading areas had elevated CH₄ fluxes compared to the corresponding vegetation types in areas that did not
275 display visual signs of degradation ($F_{8,489} = 8.15$, $P < 0.001$; $SED = 2.85 \text{ mg CH}_4 \text{ m}^{-2} \text{ h}^{-1}$), with the largest increase in
emissions being for subsiding areas of dwarf shrub (Fig 2). The emission from the subsiding tundra areas was highest in
summer corresponding to the period of highest air and soil temperatures (Fig 2 b, Fig 3). The highest emissions were from
the flooded fen vegetation types, where emissions peaked in autumn (Fig 2 c). Temperature peaked in July at the non-
flooded sites while at flooded sites temperatures remained relatively constant after the initial thaw period. The coldest
280 temperature were measured in subsiding DL and DS areas in June ($F_{8,490} = 9.06$, $P < 0.001$; $SED = 0.7 \text{ }^\circ\text{C}$).

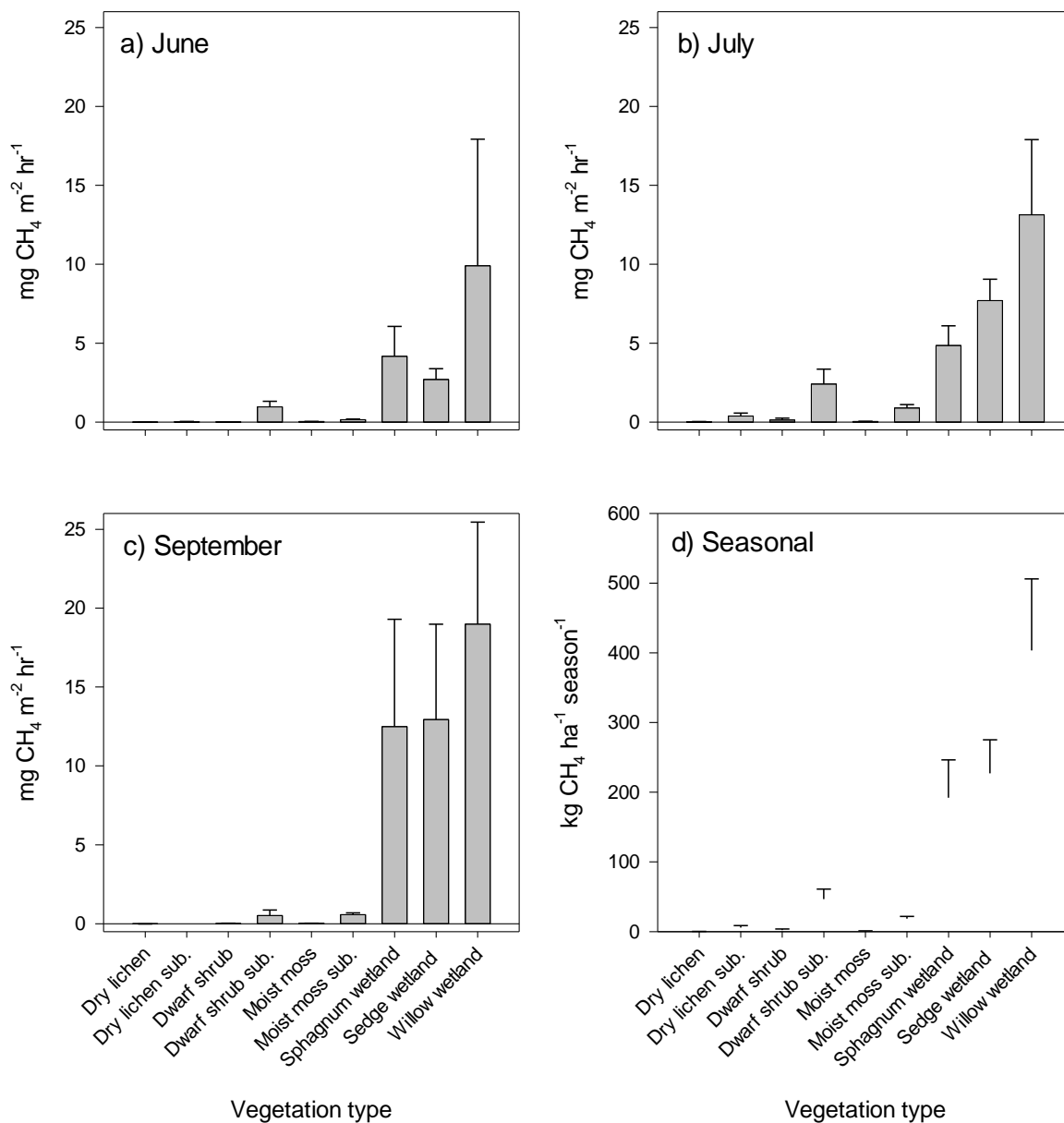
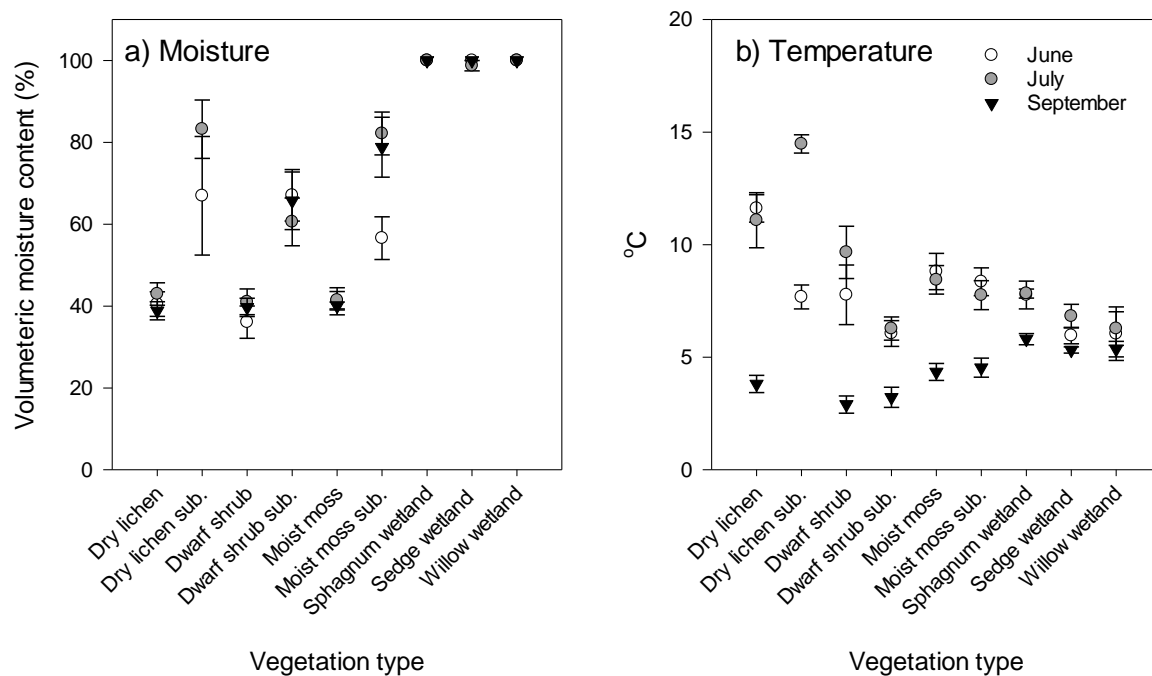


Figure 2. CH₄ fluxes measured in different vegetation types in a) June, b) July, c) September and d) cumulative seasonal CH₄ emissions, “sub.” denotes measurements made in subsiding areas of vegetation types found on the raised palsa plateaus. For September, no data are available from the dry lichen sub. class. Means and SE are shown.

Integrated CH₄ fluxes per vegetation type showed highest seasonal fluxes of ca 400 kg CH₄ ha⁻¹ season⁻¹ from willow wetland areas with emissions from *Sphagnum* and sedge wetland vegetation types being ca half those of the willow



290 areas at ca 200 kg CH₄ ha⁻¹ season⁻¹. The seasonal emissions from the subsiding dwarf shrub, moist moss, and dry lichen areas were 50 and 25 kg of CH₄ ha⁻¹ season⁻¹, respectively, which were higher than in un-degraded areas where emission from raised palsa vegetation types were low at less and/or equal to 2 kg of CH₄ ha⁻¹ season⁻¹.



295 **Figure 3. Variation in a) moisture and b) temperature among vegetation types measured in June, July and September, “sub.” denotes measurements made in subsiding areas of vegetation types found on the raised palsa plateaus. For September no data is available from the dry lichen sub. class. Means and SE are shown.**

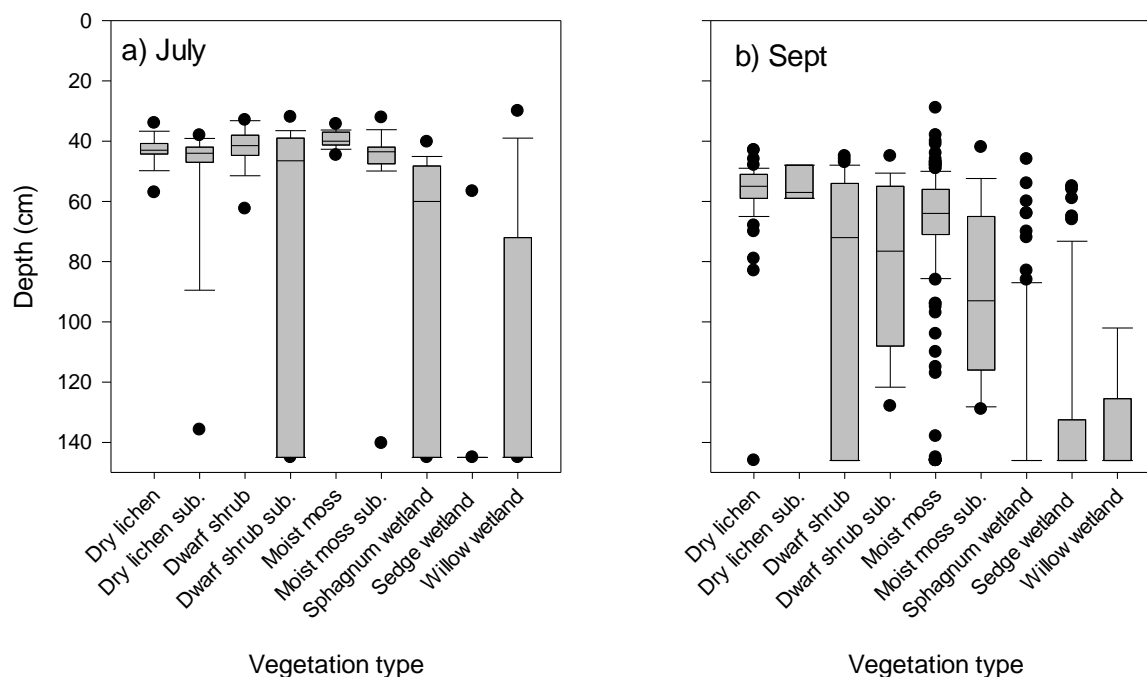


Figure 4. Variation in active layer depth among vegetation types in a) July and b) September, “sub.” denotes measurements made in subsiding areas of vegetation types found on the raised palsa plateaus.

300 3.2 Scaling CH₄ fluxes via vegetation mapping and calculation of class areal extent

The mapping of the nine vegetation classes found on degrading palsa mires using the VHR UAV data gave an overall classification accuracy of 71% (confusion matrices were generated in base R; Supplementary information 1). The area covered by the target wetland vegetation classes (i.e. excluding rock outcrops, birch forest areas, water bodies and anthropogenic surfaces) across the three sites was ca. 50 ha while the total surveyed area was 83.7 ha (Table 1). Subsequently

305 % estimates of areas are made relative to the target vegetation area. Areas where the visual inspection of the surface topography in the field clearly indicated advanced subsidence equated to 10.0 % of the area covered by the vegetation types. The three subsiding vegetation classes covered 1.5, 2.4 and 1.1 ha, or 3.0, 4.8 and 2.2 % of the target vegetation type area, for dry lichen subsiding, dwarf shrub subsiding and moist moss subsiding, respectively (Table 1). Key here was that the classification was of a high enough accuracy for this output to be used as the “ground” data for the Sentinel-2 classifications.

310

Table 1. Area of different wetland vegetation types at each of the three study sites and their proportional (Prop.) contribution to the area covered by the target vegetation types. (Please note that area of anthropogenic, exposed rock,



315 **sparse birch forest on mineral soil, forested wetland and water as well as pixels impacted by shadows are included in the CH₄ flux study and hence they are not shown in the table).**

Vegetation	Tourist St.		Storflaket		Stordalen		□ Sites (ha)
	Area (ha)	Prop (%)	Area (ha)	Prop (%)	Area (ha)	Prop (%)	
Dry lichen	0.002	0.1	0.177	1.0	0.245	0.8	0.4
Dry lichen sub	0.004	0.1	1.483	8.3	0.012	0.0	1.5
Dwarf shrub	0.494	15.0	0.897	5.0	1.785	6.1	3.2
Dwarf shrub sub	0.681	20.6	0.450	2.5	1.291	4.4	2.4
Moist moss	0.144	4.4	4.861	27.3	5.612	19.3	10.6
Moist moss sub	0.403	12.2	0.143	0.8	0.571	2.0	1.1
<i>Sphagnum</i>	0.827	25.1	2.250	12.7	7.072	24.3	10.1
Sedge	0.351	10.6	4.835	27.2	5.987	20.6	11.2
Willow	0.392	11.9	2.681	15.1	6.523	22.4	9.6
ΣTarget vegetation	3.3		17.8		29.1		50.2

320 The resultant classification vegetation maps from the Sentinel-2 hard and soft classifications had overall accuracies of 50.2% and 83.2%, respectively. The class areal extents from these classification outputs, along with class areal extents obtained when hard classification output was adjusted for misclassification bias, are presented in Table 2 (which depicts those classes shown in Table 1). The hard classification of Sentinel-2 data did not capture the fine-scale vegetation mosaic on the raised part of the palsa mire (i.e., dry lichen, and dwarf shrub prior to subsidence), instead it mapped the vegetation types in those areas as either moist moss or dwarf shrub subsiding vegetation classes, leading to the lower overall classification accuracy than obtained using the soft classification approach. Once corrected for misclassification bias, the hard classification areal extents for each vegetation class improved considerably in that the estimates are comparable to that mapped using the UAV data and the soft classification of the Sentinel-2 data. The soft classification of the Sentinel-2 data was able to map all nine target vegetation types and followed the same distribution of more or less abundant vegetation types, predicting similar total class areal extents as that of the UAV-derived maps. In both cases (bias corrected hard classification and soft classification), those vegetation types on the raised palsa area missed by the hard classification, have a calculated areal extent.

330 The soft classification of the Sentinel-2 data produced a higher estimate of the areal extent of the fen vegetation types at 35.4 ha than the UAV classification but succeeded in mapping all the vegetation classes present across the study site. The mapping from the hard classification of Sentinel-2 under-estimated the fen vegetation types slightly at 28.64 and missed some of the other vegetation classes (i.e., Dry lichen, Dry lichen subsiding and Dwarf shrub). After correcting for



335 classification bias, the areal extents of vegetation classes from the hard classification closely matched to those of the UAV
 mapped areas, with 32.21 ha of the fen vegetation types estimated to occupy the study site.

Based on the UAV-classification vegetation mapping (class areal extents), 30.9 ha (or 61%) of the area covered by
 the target vegetation types was comprised of the three vegetation classes (*Sphagnum*, sedge and willow wetland – known as
 fen vegetation types) associated with the highest CH₄ emissions. Using the mapping of areal extents from the UAV data to
 340 model CH₄ fluxes shows marked differences in CH₄ fluxes between raised palsas and the wetland types surrounding these
 (Figure 5; Table 3). Areas of the raised palsa, which are not showing visual signs of subsidence, generally have very low
 emissions while areas with degrading permafrost and subsidence, as well as those areas with no permafrost emit methane.
 Among the vegetation types that are associated with high CH₄ emissions, the maps highlight the importance of the willow
 wetland vegetation type as a source of methane from these wetlands. This is because it have both high emissions per area
 345 and covers substantial areas in particular at the Stordalen mire site. Although the highest CH₄ emissions are from the areas
 which have lost their permafrost that are surrounding the remaining palsa, there are indications of increased emissions also
 within the palsas.

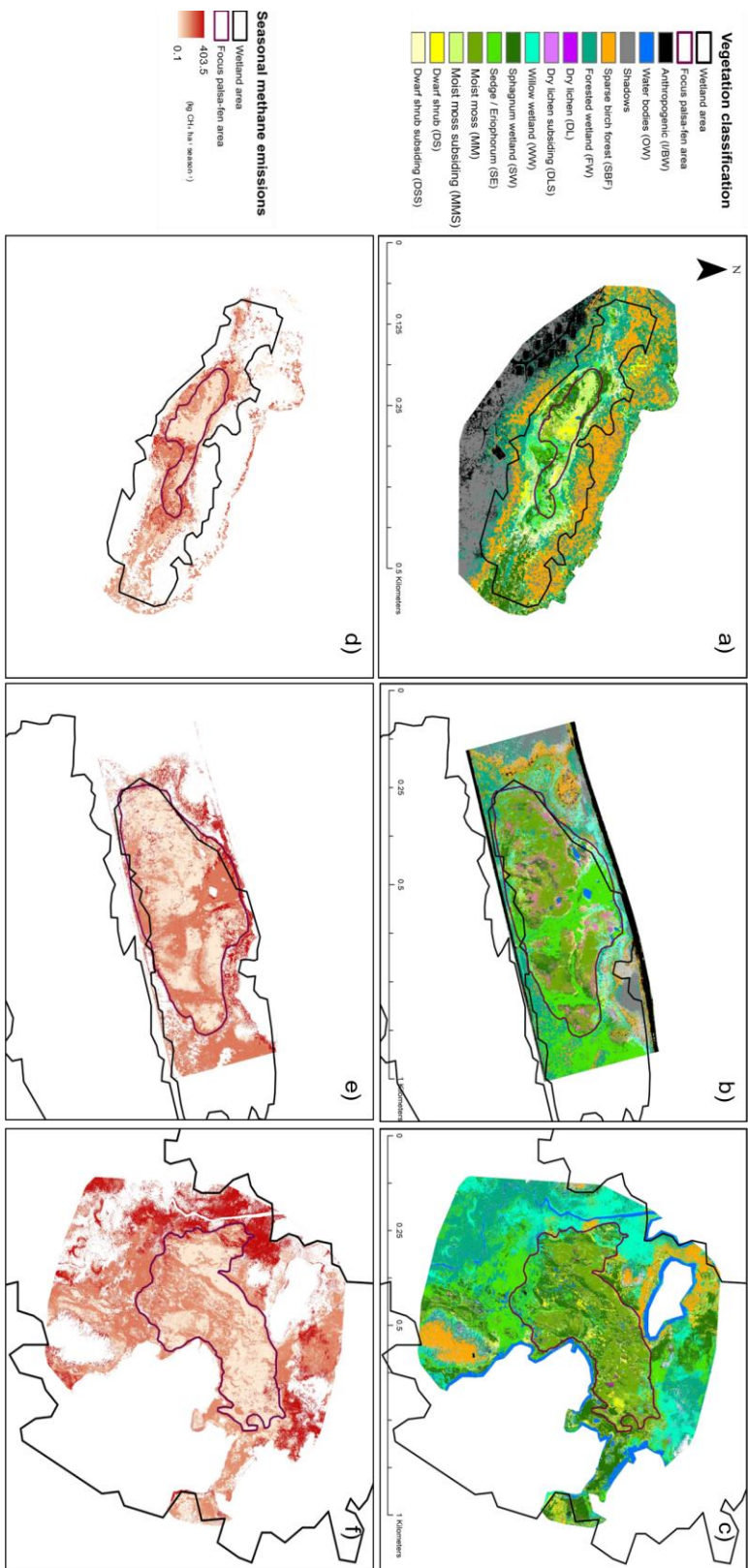
**Table 2. Comparing class areal estimates for the target vegetation types using Sentinel-2 (S-2) hard and soft
 350 classification and bias-corrected hard classification. For comparison the estimates are provided for the UAV-derived
 classification which served as the ground data.**

Vegetation type	S-2	Hard	S-2	Soft	Bias-corrected	Ground	data
	Classification	Classification	Classification	S-2	Hard	(UAV	
	Area (ha)	Area (ha)	Area (ha)	Area (ha)	Classification	Classification)	
	Area (ha)	Area (ha)	Area (ha)	Area (ha)	Area (ha)	Area (ha)	
Dry lichen	0.00	0.4	0.0	0.4			
Dry lichen sub	0.00	1.2	0.8	1.5			
Dwarf shrub	0.00	3.3	1.1	3.2			
Dwarf shrub sub	2.9	2.1	5.3	2.4			
Moist moss	13.3	8.1	13.7	10.6			
Moist moss sub	0.0	1.3	0.3	1.1			
<i>Sphagnum</i>	7.4	10.1	11.2	10.1			
Sedge	19.4	13.2	11.7	11.2			
Willow	1.8	12.1	9.3	9.6			
∑ Target vegetation	44.8	51.0	52.8	50.2			
∑ Fen with high CH₄ emission	28.6	35.4	32.2	30.9			



355 Methane emissions from within the palsa areas are commonly associated with subsiding moist moss and subsiding dwarf
shrub vegetation, as well as development of Sphagnum wetland vegetation in subsiding areas that have become waterlogged
either at the edges of the palsas or in their interior following degradation. The subsiding dwarf shrub vegetation is mainly
found along the edges of the palsas that are experiencing lateral erosion while the subsiding moist moss vegetation type
occurs in the interior parts of the palsa in areas with deeper active layers and the development of a hummocky surface.

360 When CH₄ emissions are integrated across the three wetland areas using the UAV-derived vegetation mapping net
emissions are 8519 kg CH₄ season⁻¹ (Table 3). The total emissions are composed of 16.6, 142.6 and 8359.5 kg CH₄ season⁻¹
from raised palsa vegetation (DL, DS, MM), subsiding palsa vegetation (DLS, DSS, MMS) and waterlogged vegetation
types (SW, SE WW), respectively. This shows that currently emissions from either intact areas in the early stages of
degradation is low compared to the already degraded areas. However, as the areas of raised palsa vegetation and subsiding
palsa vegetation are large (ca 20 ha (or 40% of the area covered by target vegetation types) when combined), there are
substantial risks of higher CH₄ emissions from these sites associated with continued degradation of the currently subsiding
365 areas and onset of degradation of the remaining palsa areas.





370 **Figure 5. (a-c) Detailed vegetation maps separating out wetland vegetation types including vegetation types associated with raised and subsiding palsa areas at the Tourist st., Storflaket and Stordalen mires. The vegetation maps were generated from UAV-captured data. (d-f). Maps of seasonal CH₄ emission based on the seasonal CH₄ emission measured in the nine target vegetation types across the three mire sites. The focus palsa-fen wetland area outlined in purple is the area where ground data on CH₄ fluxes were collected as well as for the vegetation mapping. The full wetland area at each site is indicated by the black boundary line.**

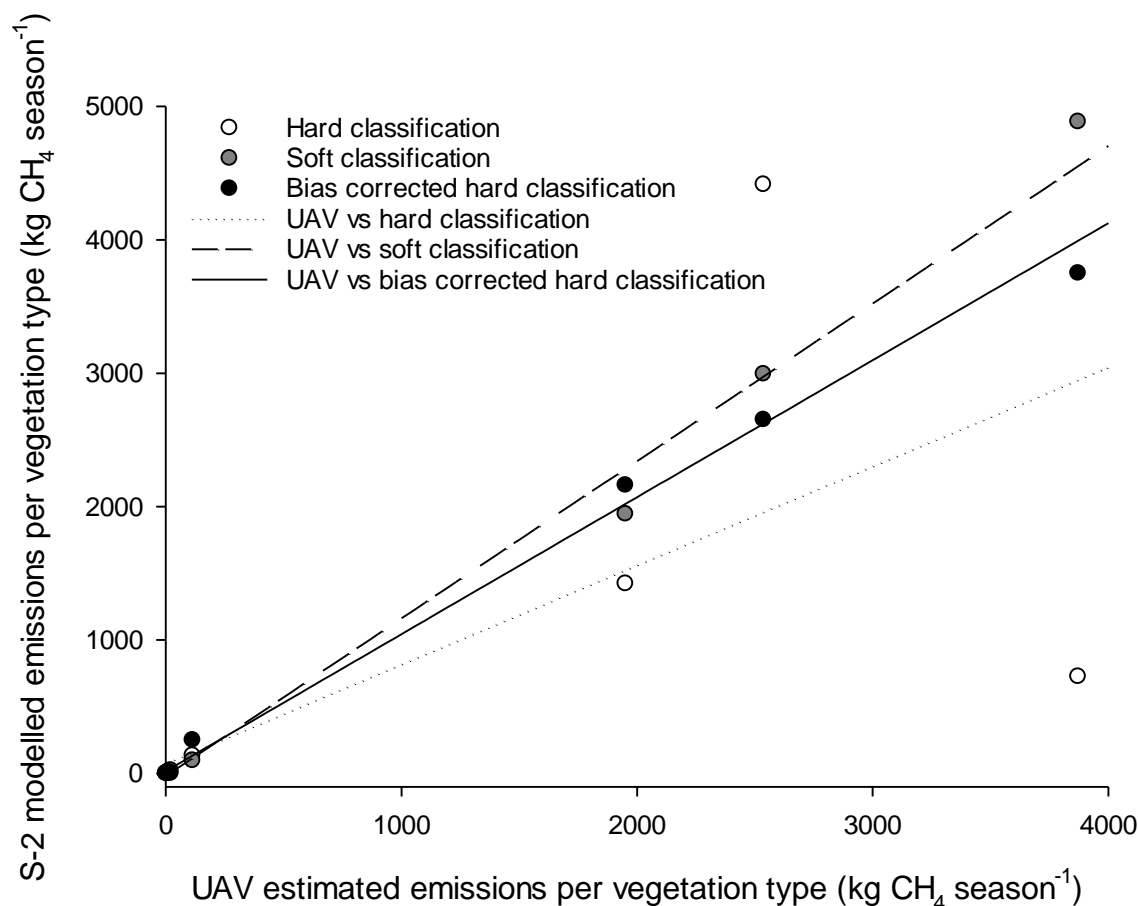
375 **Table 3. Seasonal methane emissions for 2021 for the total area of each target vegetation classes within the area covered by the UAV flights. Methane emissions are estimated using three different models using Sentinel-2 data and one model using UAV data. Mean and SE are shown.**

Vegetation	CH ₄ flux		CH ₄ flux		CH ₄ flux	
	S-2 hard classification (kg CH ₄ season ⁻¹)		S-2 soft classification (kg CH ₄ season ⁻¹)		S-2 bias corrected hard classification (kg CH ₄ season ⁻¹)	
Dry lichen	0	0	0.05	0.11	0	0
Dry lichen sub	0	0	7.2	3.6	4.7	2.3
Dwarf shrub	0	0	7.0	5.5	2.3	1.8
Dwarf shrub sub	134.5	41.4	96.7	29.7	248.6	76.4
Moist moss	12.3	3.7	7.5	2.2	12.1	3.6
Moist moss sub	0.0	0.0	23.4	4.2	4.9	0.9
<i>Sphagnum</i> wetland	1422.0	400.3	1942.8	547.0	2159.4	607.9
Sedge wetland	4415.3	936.3	2993.5	634.8	2651.8	562.3
Willow wetland	726.2	184.7	4885.9	1242.8	3750.4	953.9
∑ Vegetation types	6710		9964		8834	

380 Taking the Sentinel-2 sets of estimates of areal extent of vegetation types to estimate the CH₄ emissions of the vegetation types showed both over- and under-estimation of emissions (compared to the UAV-derived CH₄ estimates) - the hard classification under-estimated CH₄ emissions across the site by 21 %; while the soft classification over-estimated emissions by 17%. The mismatch between the Sentinel-2 hard classification and the UAV estimates were linked to a misclassification of willow wetland as sedge wetland (Table 2, Supplementary information 1). Correcting the output of the hard classification for misclassification bias improved the match of CH₄ estimates to that derived from the UAV data, and key was that target
 385 vegetation classes were included in the mapping following this post-classification process. For the soft classification, it was the misclassification of sedge and willow wetland area. Correlation analysis between the UAV- and Sentinel-2 classification outputs showed that the bias corrected hard classification was more closely correlated to the UAV predictions, followed



closely by the soft classification with $R^2 = 0.997$ and $R^2 = 0.995$ ($P < 0.001$ and $P < 0.001$), respectively. The hard classification performed least well with an $R^2 = 0.37$ ($P < 0.001$; Fig 6).

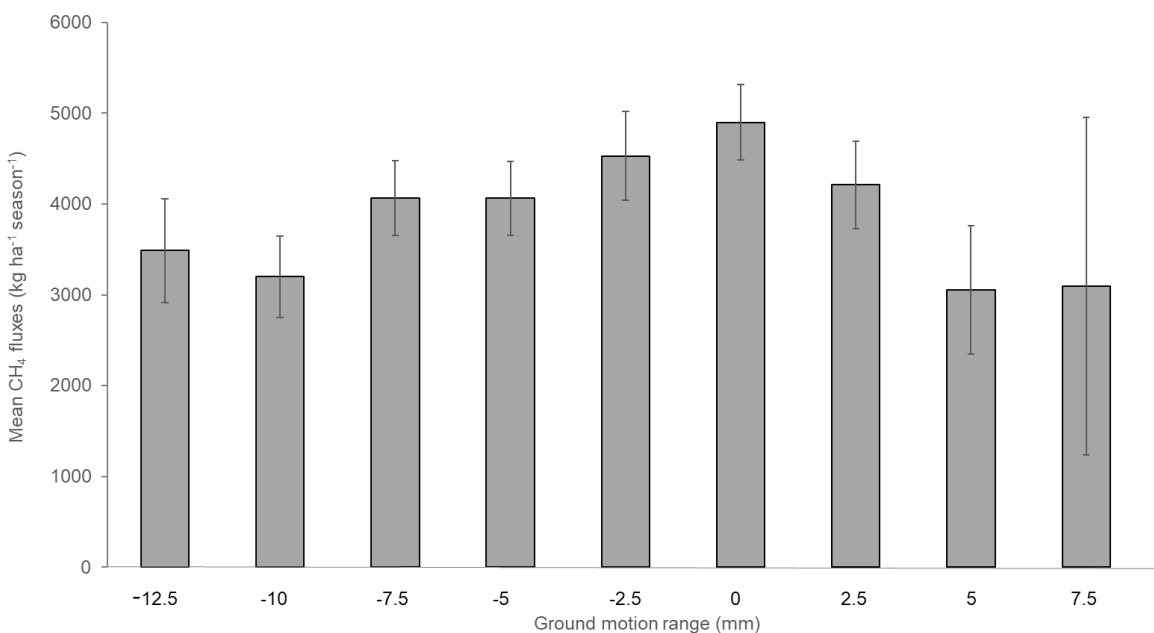


390

Figure 6. Relationship between UAV estimated methane emissions per vegetation types and the three Sentinel-2 (S-2) models.

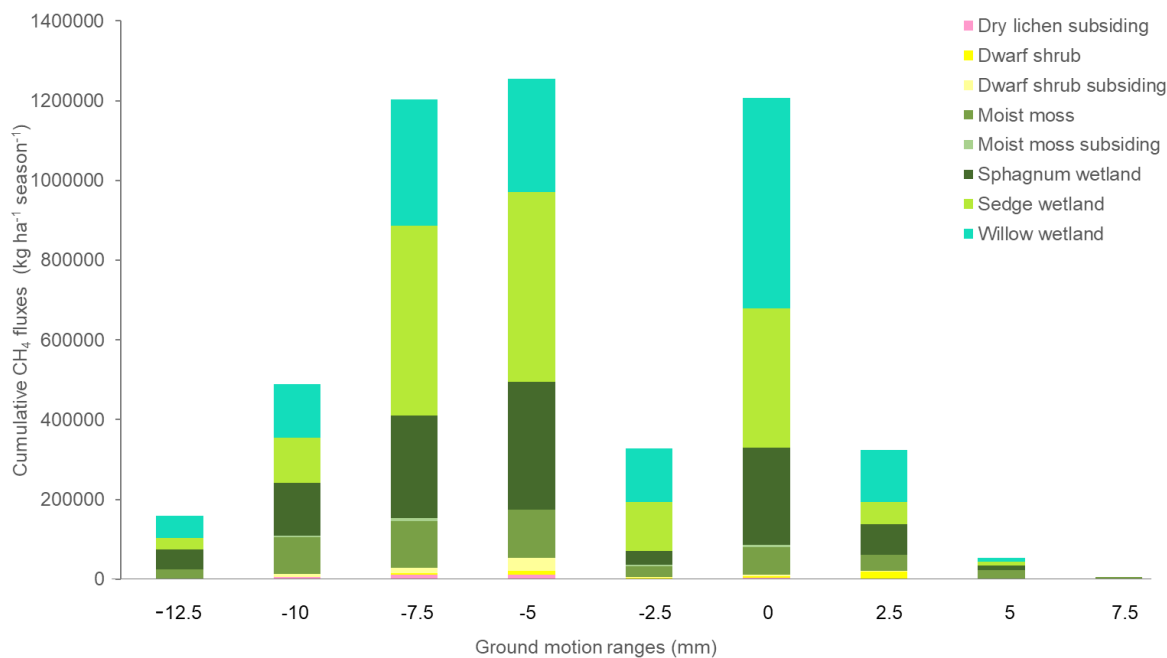
3.3 Linking InSAR determined ground motion to CH₄ emissions

395 InSAR detected subsidence across 90 % of the study area, indicating that the majority of the surface of these sites were impacted by mm level rates of subsidence. However, rates of ground motion varied considerably across the study area and among vegetation types. Importantly, across the three sites, areas with relatively low levels of ground motion were associated with the highest mean CH₄ emissions ($F_{8,1135} = 5.63$, $p < 0.001$, $SED = 961.5$; Fig 6) while both uplifting and the most subsiding areas tended to have lower fluxes. High cumulative CH₄ emissions (summed over all pixels for a given range of ground motions) were found for areas that were either stable or subsiding at an intermediate rate (Fig 7) while the most
400 subsiding areas had low cumulative CH₄ emissions.



405 **Figure 7. Average seasonal CH₄ emissions for different ground motion ranges (categories in 2.5 mm ranges) across the three study sites. Negative values indicate subsidence and positive values indicate uplift. Mean and SE are shown.**

This pattern of areas of high subsidence being linked to areas of low CH₄ emissions was also apparent in the subsidence and CH₄ emissions maps (Fig 9). For example, at the Tourist St. mire areas of high subsidence (comprising mainly subsiding moist moss vegetation Fig 5 a) corresponded to areas with relatively low CH₄ emissions while areas that have already
410 transitioned to *Sphagnum* or willow wetland are associated with bands of high CH₄ emissions along the degrading edge of the palsa plateaux (Fig 5 a and d). Similar patterns were evident on the Storflaket mire, where degrading areas within the palsa plateaux did not display high CH₄ emissions while areas that have transitions to *Sphagnum* or sedge wetland have high CH₄ emissions (Fig 7 b and e). The Stordalen site showed the largest areas of high subsidence that traversed the boundary
415 between the palsa plateau and the fen areas (Fig 7 c and f). In this part of Stordalen the *Sphagnum* wetland vegetation type was present both in the hollows in the degrading interior of the palsa plateaux and in adjacent areas where the palsas had already collapsed, explaining the high CH₄ emissions (together with the presence of the willow wetland vegetation type) from this area.



420

Figure 8. Cumulative CH₄ emission (\pm SE) for different ground motions across the thaw seasons of 2017 and 2020 for pixels (i.e. a sum of the CH₄ emissions from all pixel of a given ground motion (categories in 2.5 mm ranges)) of the target vegetation classes. The dry lichen vegetation types did not cover large enough areas to be evaluated on the 20×20 m pixel scale of the ground motion data and is therefore not included in this comparison. Negative values indicate subsidence and positive values indicate uplift.

425

The net emissions of CH₄ across subsiding parts of the three wetlands (as detected by InSAR) were modest at 116 kg CH₄ season⁻¹. However, when these areas have degraded to such a point that they are fully waterlogged and have transitioned to either *Sphagnum* or sedge vegetation we estimate emissions from these, currently low emitting, areas to be around 6480 kg season⁻¹ or if we use the highest emitting vegetation type as a predictor of future emissions we arrive at 12 960 kg season⁻¹.

430

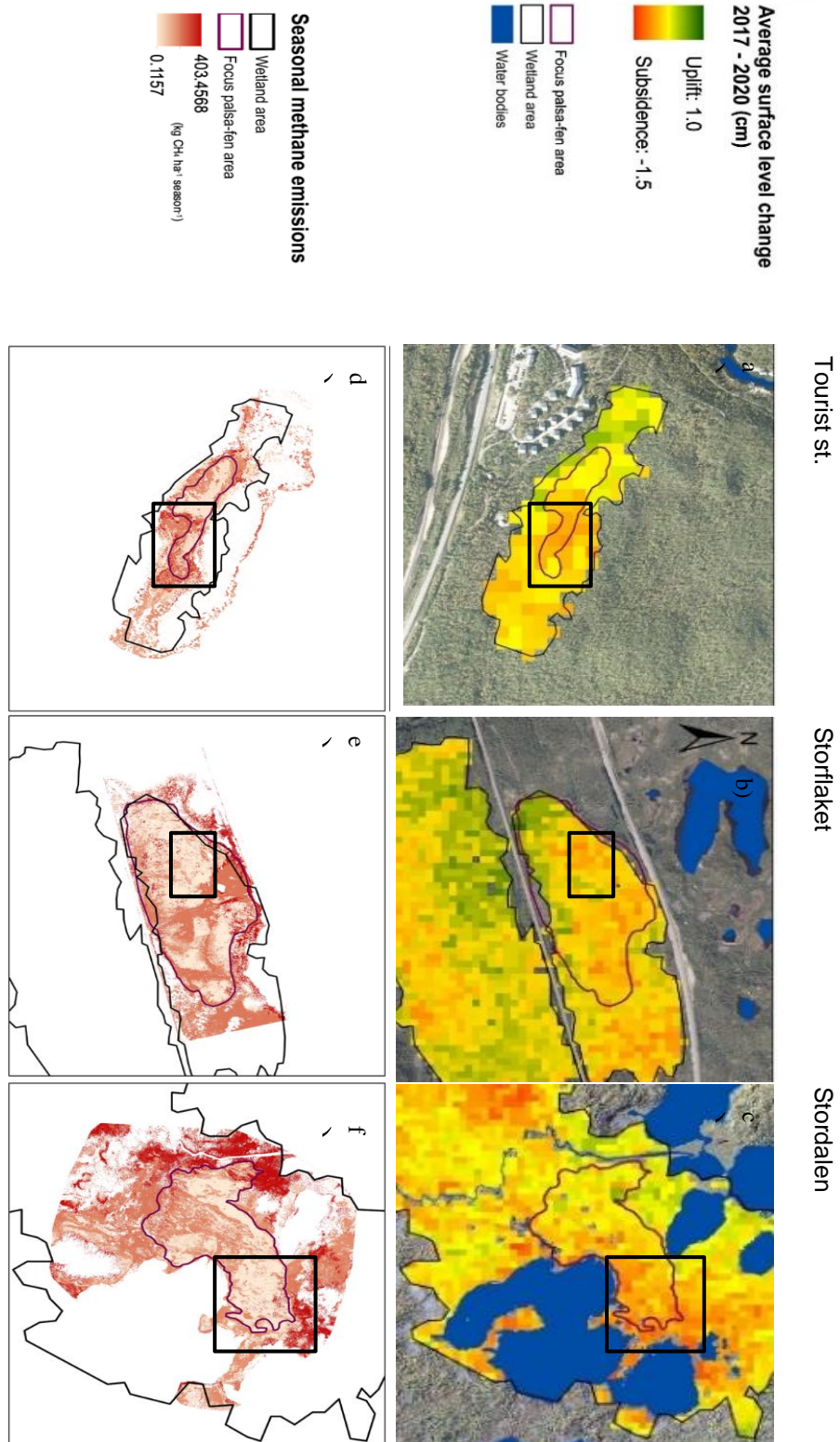




Figure 9. Maps of (a-c) ground motion (de la Bautista Barred et al., 2022) and (d-f) CH₄ fluxes at the Toursist st., Storflaket, and Stordalen mire. The black boxes show the areas referred to in the text.

435

4 Discussion

Methane emissions varied strongly across the palsa peatlands with consistent differences among vegetation types over space and time. The low emissions from the intact dry palsa areas and trends of increased emission following degradation and flooding were comparable with those reported from other part of Scandinavia and Russia (Nykänen et al., 2003; Olefeldt et al., 2013; Liebner et al., 2015; Miglovets et al., 2021; Varner et al., 2022; Glagolev et al., 2011). However, there was strong variation in the magnitude of that response depending on the degradation stage, level of flooding and vegetation community present. For example, as long as sites were mainly impacted by increased waterlogging but no vegetation change (i.e. the raised palsa vegetation persisted despite experiencing subsidence), CH₄ emissions only increased modestly (Fig 2). This suggest that waterlogging *per se* was not sufficient to drive high emissions as these were only recorded following flooding and a transition of the vegetation community to *Sphagnum* mosses, sedges and other wetland adapted species. This is consistent with the literature where different type of sedge vegetation communities and thermokarst activity were associated with the higher end of emissions (Glagolev et al., 2011; Dzyuban, 2002; Walter et al., 2006). An important finding here is the high CH₄ emissions reported from fen and in particular the willow vegetation type. These emissions were consistent across the three study sites and were at the upper range of emissions reported in the literature (Olefeldt et al., 2013; Miglovets et al., 2021) and in the range of emissions from ponds and thermokarst lakes in degrading permafrost in the literature (Walter et al., 2006; Glagolev et al., 2011; Dzyuban, 2002). Possible explanations for this variation among vegetation types and very high CH₄ emissions are the impact of the vegetation on CH₄ emission both via plant mediated transport, root exudate quality and quantity and the level of rhizosphere oxidation. For example, both *M. trifoliata* and in particular *C. rupestris* are known to transport CH₄ through their vascular tissues while other species common in our system e.g. *S. lapponica* do not share this trait (Ge, 2022). An additional way in which plants may contribute to high CH₄ production and emissions are by releasing labile carbon in the form of root exudates into the rhizosphere. This carbon flow can represent a substantial part of NPP and can have a large impact on CH₄ emissions (Ström et al., 2003; Girkin, 2018). We speculate that some of the willow vegetation type species, *S. lapponica*, and other *Salix* ssp, and *Comarum palustre*, which were abundant within the willow wetland vegetation type, may drive high emissions via root exudation or those species may reflect specific edaphic conditions that are favourable for CH₄ production. Further, root exudation may be an explanation of high emissions also from the tall sedge vegetation type. However, further studies would be required to establish if the high emissions from the willow wetland vegetation community in our study is consistent across greater spatial ranges as well as the specific drivers of the high emissions. Given the variation in flux rates among areas with different vegetation types, despite broadly similar moisture conditions, it is also likely that the species composition within the wide vegetation classes often used for describing permafrost peatlands (raised palsa and fen) directly impact the magnitude of the CH₄ emissions as these peatlands

465
22



degrade. Hence improved understanding the plant species specific mechanisms that control CH₄ emissions beyond abiotic drivers (such as water logging, redox, soil and air temperature) (Olefeldt et al., 2013) are important for estimations of landscape level CH₄ emission and how these will be altered as these palsa peatlands continue to degrade and their vegetation composition change.

The fact that small extents and local-scale variation in ground/vegetation conditions strongly impact net emissions is important when it comes to developing spatial models for predicting CH₄ emissions over large areas. Our three models using Sentinel-2 data differed in their ability to detect the local-scale variation in the vegetation. The hard classification model did not succeed in capturing this variability and underestimated the total wetland area. The soft and adjusted hard classification was both successful in estimating the overall area of the target vegetation types compared to the UAV estimated areas. When the areal estimates from the three models were used for extrapolating the CH₄ emissions only the adjusted hard classification estimated the emissions within a 5% error margin to the UAV estimated fluxes. The hard classification underestimated fluxes by 21 % while the soft classification over estimated emissions with 17%. This means that Sentinel-2 (or other freely available satellite data products e.g. Landsat) have sufficient spatial resolution to be an effective tools for scaling up CH₄ emissions linked to particular vegetation types in the local scale vegetation mosaic that composes degrading peatland. However, among the three Sentinel-2 models we used, the adjusted hard classification clearly outperformed the other two models. Both, the unadjusted hard or soft classification, would have included considerable error when used to extrapolate the emissions to regional scale due to scale-dependency leading to inaccuracy in the relative distribution of individual land cover classes at coarser resolutions (Siewert, 2018; Hugelius et al., 2020). This highlights both the risks of substantially increasing the error of the modelled estimates and the opportunity offered by the adjusted hard classification approach for scaling of CH₄ emissions using remotes sensing data (Olofsson et al., 2013; Olofsson et al., 2014).

The implication of this is that current estimates of changes in GHG emissions following permafrost degradation that often only use the distinction between palsa and fen (e.g. (Nykänen et al., 2003; Olefeldt et al., 2013; Miglovets et al., 2021; Varner et al., 2022) may result in considerable uncertainty and substantial underestimation of CH₄ emissions linked to degradation. This is because although this simple classification will reflect the major shift from dry to wet conditions and the large increase in CH₄ emissions that are associated with this, hot spots of high emissions will be missed as well as variation in CH₄ emissions among different fen vegetation types. The role of different vegetation types is evident from our CH₄ data from a range of wetland vegetation communities found at the study sites. These shows that variation in CH₄ emissions among common vegetation types within the “fen” vegetation class can result in nearly twice as high emissions on an areal basis. Here the detailed vegetation mapping capabilities of drones provide an important way forward together with higher resolution aerial photography and satellite data e.g. WorldView, Quickbird, and Planet Ltd’s “Super Dove mission when upscaling plot data to the landscape scale (Siewert and Olofsson, 2020; Siewert et al., 2015).

The relatively low CH₄ emissions from areas with high subsidence (Fig 7-9) reflect both the fact that they (i) represent the permafrost degradation front, which is spatially less extensive than already degraded or stable areas, and (ii)



that although the subsiding areas of a given vegetation type (Fig 2) release more CH₄ than their intact counter parts, emissions are low compared to areas which are fully degraded and flooded. Further, although CH₄ emissions increased as a specific vegetation types showed signs of permafrost degradation and subsidence (Fig 2) the initial increase in CH₄ emissions at the most subsiding sites is modest compared to the high CH₄ emissions in areas where degradation has progressed to a point where permafrost has thawed all together and subsidence has slowed down (albeit some consolidation of the peat material is still ongoing as suggested by subsidence rates at a lower rate in areas which have lost their permafrost).

Our work suggest that subsidence measured using ASPIS-InSAR can be used to predict increases in CH₄ emissions from areas experiencing permafrost degradation. The InSAR method also offers a highly sensitive early warning system of the initial stages of degradation. This is valuable because early stages of permafrost degradation are difficult to capture using optical data or ground surveys, which tend to rely on changes in the vegetation or increased surface heterogeneity which only become apparent after the degradation has progressed substantially. This is evident in the different areal estimates of the subsiding area using the two different vegetation mapping approaches using UAV and Sentinel 2 data. Mapping for subsiding areas using ground truthing of VHR UAV optical data estimated the subsiding area of the study sites to ca 10% while the InSAR data detected subsidence in 90% of the wetland area. The implication of the InSAR data is that the majority of the palsa peatlands area at our study sites is already experiencing permafrost degradation. Indeed, ongoing large-scale permafrost degradation at the sites is further supported by analysis of historical orthophotos and long term satellite data analysis as well as model predictions that suggest that permafrost in wetland will no longer be supported in northern Scandinavia by 2050 (De La Barreda-Bautista et al., 2022; Varner et al., 2022; Fewster et al., 2022). This raises concerns for the fate of the ca 2000 ha of palsa peatlands in Sweden over the next decades (Backe, 2014). The evidence of large-scale degradation at our study sites and the potential for very high CH₄ emissions from areas that currently have low emissions are a serious risk linked to climate heating in northern Scandinavia and highlights the need for regional estimates of the potential for increased CH₄ emissions associated with degradation of palsa peatlands.

Acknowledgements

We are grateful for the field work support from Mattias Dalkvist, Veronica Escubar Ruiz, and staff at Abisko Scientific Research Station. We also acknowledge that the climate data evaluation has been made by data provided by Abisko Scientific Research Station and the Swedish Infrastructure for Ecosystem Science (SITES). We are grateful to Samuel Valman for advice on data processing.

Supplementary information

Supplementary information 1. Excel file containing confusion matrixes for the hard and soft classifications.



535 References

- Åkerman, H. J. and Johansson, M.: Thawing permafrost and thicker active layers in sub-arctic Sweden, *Permafrost and Periglacial Processes*, 19, 279-292, <https://doi.org/10.1002/ppp.626>, 2008.
- 540 Alshammari, L., Large, D. J., Boyd, D. S., Sowter, A., Anderson, R., Andersen, R., and Marsh, S.: Long-Term Peatland Condition Assessment via Surface Motion Monitoring Using the ISBAS DInSAR Technique over the Flow Country, Scotland, *Remote Sensing*, 10, 10.3390/rs10071103, 2018.
- Alshammari, L., Boyd, D. S., Sowter, A., Marshall, C., Andersen, R., Gilbert, P., Marsh, S., and Large, D. J.: Use of Surface
545 Motion Characteristics Determined by InSAR to Assess Peatland Condition, *Journal of Geophysical Research: Biogeosciences*, 125, e2018JG004953, <https://doi.org/10.1029/2018JG004953>, 2020.
- Backe, S.: *Kartering av Sveriges palsmyrar*, Länsstyrelsen 2014.
- 550 Ballantyne C. K.: *Periglacial geomorphology*, John Wiley & Sons 2018.
- Biskaborn, B. K., Smith, S. L., Noetzi, J., Matthes, H., Vieira, G., Streletskiy, D. A., Schoeneich, P., Romanovsky, V. E., Lewkowicz, A. G., Abramov, A., Allard, M., Boike, J., Cable, W. L., Christiansen, H. H., Delaloye, R., Diekmann, B., Drozdov, D., Etzelmüller, B., Grosse, G., Guglielmin, M., Ingeman-Nielsen, T., Isaksen, K., Ishikawa, M., Johansson, M.,
555 Johannsson, H., Joo, A., Kaverin, D., Kholodov, A., Konstantinov, P., Kröger, T., Lambiel, C., Lanckman, J.-P., Luo, D., Malkova, G., Meiklejohn, I., Moskalenko, N., Oliva, M., Phillips, M., Ramos, M., Sannel, A. B. K., Sergeev, D., Seybold, C., Skryabin, P., Vasiliev, A., Wu, Q., Yoshikawa, K., Zheleznyak, M., and Lantuit, H.: Permafrost is warming at a global scale, *Nature Communications*, 10, 264, 10.1038/s41467-018-08240-4, 2019.
- Borge, A. F., Westermann, S., Solheim, I., and Etzelmüller, B.: Strong degradation of palsas and peat plateaus in northern
560 Norway during the last 60 years, *The Cryosphere*, 11, 1-16, 10.5194/tc-11-1-2017, 2017.
- Bradley, A. V., Andersen, R., Marshall, C., Sowter, A., and Large, D. J.: Identification of typical eco-hydrological behaviours using InSAR allows landscape-scale mapping of peatland condition, *Earth Surf. Dynam. Discuss.*, 2021, 1-28, 10.5194/esurf-2021-58, 2021.
- 565 Chadburn, S. E., Burke, E. J., Cox, P. M., Friedlingstein, P., Hugelius, G., and Westermann, S.: An observation-based constraint on permafrost loss as a function of global warming, *Nature Climate Change*, 7, 340-344, 10.1038/nclimate3262, 2017.



- 570 Cigna, F. and Sowter, A.: The relationship between intermittent coherence and precision of ISBAS InSAR ground motion velocities: ERS-1/2 case studies in the UK, *Remote Sensing of Environment*, 202, 177-198, <https://doi.org/10.1016/j.rse.2017.05.016>, 2017.
de la Barreda-Bautista, B., Boyd, D. S., Ledger, M., Siewert, M. B., Chandler, C., Bradley, A.
- 575 V., Gee, D., Large, D. J., Olofsson, J., Sowter, A., and Sjögersten, S.: Towards a Monitoring Approach for Understanding Permafrost Degradation and Linked Subsidence in Arctic Peatlands, 10.3390/rs14030444, 2022.
- Dzyuban, A.: Intensity of the microbiological processes of the methane cycle in different types of Baltic lakes, *Microbiology*, 71, 98-104, 2002.
- 580 Euskirchen, E. S., Edgar, C. W., Turetsky, M. R., Waldrop, M. P., and Harden, J. W.: Differential response of carbon fluxes to climate in three peatland ecosystems that vary in the presence and stability of permafrost, *Journal of Geophysical Research: Biogeosciences*, 119, 1576-1595, <https://doi.org/10.1002/2014JG002683>, 2014.
- 585 Fewster, R. E., Morris, P. J., Ivanovic, R. F., Swindles, G. T., Peregon, A. M., and Smith, C. J.: Imminent loss of climate space for permafrost peatlands in Europe and Western Siberia, *Nature Climate Change*, 12, 373-379, 10.1038/s41558-022-01296-7, 2022.
- 590 Foody, G. M. and Mathur, A.: A relative evaluation of multiclass image classification by support vector machines, *IEEE Transactions on Geoscience and Remote Sensing*, 42, 1335-1343, 10.1109/TGRS.2004.827257, 2004.
- Ge, M., Koskinen, M., Korrensalo, A., Mäkiranta, P., Lohila, A., and Pihlatie, M.: Species-specific effects of vascular plants on methane transport in northern peatlands, *EGU General Assembly 2022, Vienna, Austria, 23–27 May 2022*, <https://doi.org/10.5194/egusphere-egu22-2574>, 2022.,
- 595 Gee, D., Bateson, L., Sowter, A., Grebby, S., Novellino, A., Cigna, F., Marsh, S., Banton, C., and Wyatt, L.: Ground Motion in Areas of Abandoned Mining: Application of the Intermittent SBAS (ISBAS) to the Northumberland and Durham Coalfield, UK, *Geosciences*, 7, 10.3390/geosciences7030085, 2017.
- 600 Girkin, N. T.: Tropical forest greenhouse gas emissions: root regulation of soil processes and fluxes, University of Nottingham, 2018.



- Glagolev, M., Kleptsova, I., Filippov, I., Maksyutov, S., and Machida, T.: Regional methane emission from West Siberia mire landscapes, *Environmental Research Letters*, 6, 045214, 2011.
- 605
- Grosse, G., Goetz, S., McGuire, A. D., Romanovsky, V. E., and Schuur, E. A. G.: Changing permafrost in a warming world and feedbacks to the Earth system, *Environmental Research Letters*, 11, 040201, [10.1088/1748-9326/11/4/040201](https://doi.org/10.1088/1748-9326/11/4/040201), 2016.
- Hugelius, G. A.-O., Loisel, J. A.-O., Chadburn, S. A.-O. X., Jackson, R. A.-O., Jones, M. A.-O., MacDonald, G.,
610 Marushchak, M., Olefeldt, D. A.-O., Packalen, M., Siewert, M. A.-O., Treat, C. A.-O., Turetsky, M., Voigt, C. A.-O., and Yu, Z. A.-O.: Large stocks of peatland carbon and nitrogen are vulnerable to permafrost thaw, 2020.
- Johansson, M., Callaghan, T. V., Bosiö, J., Åkerman, H. J., Jackowicz-Korczynski, M., and Christensen, T. R.: Rapid responses of permafrost and vegetation to experimentally increased snow cover in sub-arctic Sweden, *Environmental*
615 *Research Letters*, 8, 035025, [10.1088/1748-9326/8/3/035025](https://doi.org/10.1088/1748-9326/8/3/035025), 2013.
- Liebner, S., Ganzert, L., Kiss, A., Yang, S., Wagner, D., and Svenning, M. M.: Shifts in methanogenic community composition and methane fluxes along the degradation of discontinuous permafrost, *Frontiers in Microbiology*, 6, 356, 2015.
- 620 Luoto, M. and Seppälä, M.: Thermokarst ponds as indicators of the former distribution of palsas in Finnish Lapland, *Permafrost and Periglacial Processes*, 14, 19-27, <https://doi.org/10.1002/ppp.441>, 2003.
- Maksyutov, S., Glagolev, M., Kleptsova, I., Sabrekov, A., Peregon, A., and Machida, T.: Methane emissions from the West Siberian wetlands, *AGU Fall Meeting Abstracts*, GC41D-02,
- 625
- McGuire, A. D., Anderson, L. G., Christensen, T. R., Dallimore, S., Guo, L., Hayes, D. J., Heimann, M., Lorenson, T. D., Macdonald, R. W., and Roulet, N.: Sensitivity of the Carbon Cycle in the Arctic to Climate Change, *Ecological Monographs*, 79, 523-555, 2009.
- 630 Miglovets, M., Zagirova, S., Goncharova, N., and Mikhailov, O.: Methane Emission from Palsa Mires in Northeastern European Russia, *Russian Meteorology and Hydrology*, 46, 52-59, 2021.
- Mishra, U., Hugelius, G., Shelef, E., Yang, Y., Strauss, J., Lupachev, A., Harden Jennifer, W., Jastrow Julie, D., Ping, C.-L., Riley William, J., Schuur Edward, A. G., Matamala, R., Siewert, M., Nave Lucas, E., Koven Charles, D., Fuchs, M.,
635 Palmtag, J., Kuhry, P., Treat Claire, C., Zubrzycki, S., Hoffman Forrest, M., Elberling, B., Camill, P., Veremeeva, A., and



- Orr, A.: Spatial heterogeneity and environmental predictors of permafrost region soil organic carbon stocks, *Science Advances*, 7, eaaz5236, 10.1126/sciadv.aaz5236, 2021.
- 640 Nykänen, H., Heikkinen, J. E., Pirinen, L., Tiilikainen, K., and Martikainen, P. J.: Annual CO₂ exchange and CH₄ fluxes on a subarctic palsamire during climatically different years, *Global biogeochemical cycles*, 17, 2003.
- Olefeldt, D., Turetsky, M. R., Crill, P. M., and McGuire, A. D.: Environmental and physical controls on northern terrestrial methane emissions across permafrost zones, *Global change biology*, 19, 589-603, 2013.
- 645 Olefeldt, D., Roulet, N. T., Bergeron, O., Crill, P., Bäckstrand, K., and Christensen, T. R.: Net carbon accumulation of a high-latitude permafrost palsamire similar to permafrost-free peatlands, *Geophysical Research Letters*, 39, 2012.
- Olofsson, P., Foody, G. M., Stehman, S. V., and Woodcock, C. E.: Making better use of accuracy data in land change studies: Estimating accuracy and area and quantifying uncertainty using stratified estimation, *Remote Sensing of Environment*, 129, 122-131, <https://doi.org/10.1016/j.rse.2012.10.031>, 2013.
- 650 Olofsson, P., Foody, G. M., Herold, M., Stehman, S. V., Woodcock, C. E., and Wulder, M. A.: Good practices for estimating area and assessing accuracy of land change, *Remote Sensing of Environment*, 148, 42-57, <https://doi.org/10.1016/j.rse.2014.02.015>, 2014.
- 655 Olvmo, M., Holmer, B., Thorsson, S., Reese, H., and Lindberg, F.: Sub-arctic palsamire degradation and the role of climatic drivers in the largest coherent palsamire complex in Sweden (Vissátvuopmi), 1955–2016, *Scientific Reports*, 10, 8937, 10.1038/s41598-020-65719-1, 2020.
- 660 Sannel, A. B. K. and Kuhry, P.: Warming-induced destabilization of peat plateau/thermokarst lake complexes, *Journal of Geophysical Research: Biogeosciences*, 116, <https://doi.org/10.1029/2010JG001635>, 2011.
- Sannel, A. B. K., Hugelius, G., Jansson, P., and Kuhry, P.: Permafrost Warming in a Subarctic Peatland – Which Meteorological Controls are Most Important?, *Permafrost and Periglacial Processes*, 27, 177-188, <https://doi.org/10.1002/ppp.1862>, 2016.
- 665 Schneider von Deimling, T., Meinshausen, M., Levermann, A., Huber, V., Frieler, K., Lawrence, D. M., and Brovkin, V.: Estimating the near-surface permafrost-carbon feedback on global warming, *Biogeosciences*, 9, 649-665, 10.5194/bg-9-649-2012, 2012.



670

Schuur, E. A. G. and Abbott, B.: High risk of permafrost thaw, *Nature*, 480, 32-33, 10.1038/480032a, 2011.

Siewert, M. B.: High-resolution digital mapping of soil organic carbon in permafrost terrain using machine learning: a case study in a sub-Arctic peatland environment, *Biogeosciences*, 15, 1663-1682, 10.5194/bg-15-1663-2018, 2018.

675

Siewert, M. B. and Olofsson, J.: Scale-dependency of Arctic ecosystem properties revealed by UAV, *Environmental Research Letters*, 15, 094030, 10.1088/1748-9326/aba20b, 2020.

Siewert, M. B., Lantuit, H., Richter, A., and Hugelius, G.: Permafrost Causes Unique Fine-Scale Spatial Variability Across Tundra Soils, *Global Biogeochemical Cycles*, 35, e2020GB006659, <https://doi.org/10.1029/2020GB006659>, 2021.

680

Siewert, M. B., Hanisch, J., Weiss, N., Kuhry, P., Maximov, T. C., and Hugelius, G.: Comparing carbon storage of Siberian tundra and taiga permafrost ecosystems at very high spatial resolution, *Journal of Geophysical Research: Biogeosciences*, 120, 1973-1994, <https://doi.org/10.1002/2015JG002999>, 2015.

685

Sjöberg, Y., Marklund, P., Pettersson, R., and Lyon, S. W.: Geophysical mapping of palsa peatland permafrost, *The Cryosphere*, 9, 465-478, 10.5194/tc-9-465-2015, 2015.

Sjöberg, Y., Siewert, M. B., Rudy, A. C. A., Paquette, M., Bouchard, F., Malenfant-Lepage, J., and Fritz, M.: Hot trends and impact in permafrost science, *Permafrost and Periglacial Processes*, 31, 461-471, <https://doi.org/10.1002/ppp.2047>, 2020.

690

Sjögersten, S., Caul, S., Daniell, T. J., Jurd, A. P. S., O'Sullivan, O. S., Stapleton, C. S., and Titman, J. J.: Organic matter chemistry controls greenhouse gas emissions from permafrost peatlands, *Soil Biology and Biochemistry*, 98, 42-53, <https://doi.org/10.1016/j.soilbio.2016.03.016>, 2016.

695

Sowter, A., Bin Che Amat, M., Cigna, F., Marsh, S., Athab, A., and Alshammari, L.: Mexico City land subsidence in 2014–2015 with Sentinel-1 IW TOPS: Results using the Intermittent SBAS (ISBAS) technique, *International Journal of Applied Earth Observation and Geoinformation*, 52, 230-242, <https://doi.org/10.1016/j.jag.2016.06.015>, 2016.

700

Ström, L., Ekberg, A., Mastepanov, M., and Røjle Christensen, T.: The effect of vascular plants on carbon turnover and methane emissions from a tundra wetland, *Global Change Biology*, 9, 1185-1192, <https://doi.org/10.1046/j.1365-2486.2003.00655.x>, 2003.



- 705 Tarnocai, C., Canadell, J. G., Schuur, E. A. G., Kuhry, P., Mazhitova, G., and Zimov, S.: Soil organic carbon pools in the northern circumpolar permafrost region, *Global Biogeochemical Cycles*, 23, <https://doi.org/10.1029/2008GB003327>, 2009.
- Turetsky, M. R., Abbott, B. W., Jones, M. C., Anthony, K. W., Olefeldt, D., Schuur, E. A. G., Grosse, G., Kuhry, P., Hugelius, G., Koven, C., Lawrence, D. M., Gibson, C., Sannel, A. B. K., and McGuire, A. D.: Carbon release through abrupt permafrost thaw, *Nature Geoscience*, 13, 138-143, 10.1038/s41561-019-0526-0, 2020.
- 710 van Huissteden, J., Teshebaeva, K., Cheung, Y., Magnússon, R. Í., Noorbergen, H., Karsanaev, S. V., Maximov, T. C., and Dolman, A. J.: Geomorphology and InSAR-Tracked Surface Displacements in an Ice-Rich Yedoma Landscape, *Frontiers in Earth Science*, 9, 10.3389/feart.2021.680565, 2021.
- 715 Varner, R. K., Crill, P. M., Frohling, S., McCalley, C. K., Burke, S. A., Chanton, J. P., Holmes, M. E., null, n., Saleska, S., and Palace, M. W.: Permafrost thaw driven changes in hydrology and vegetation cover increase trace gas emissions and climate forcing in Stordalen Mire from 1970 to 2014, *Philosophical Transactions of the Royal Society A: Mathematical, Physical and Engineering Sciences*, 380, 20210022, 10.1098/rsta.2021.0022, 2022.
- 720 Walter Anthony, K., Daanen, R., Anthony, P., Schneider von Deimling, T., Ping, C.-L., Chanton, J. P., and Grosse, G.: Methane emissions proportional to permafrost carbon thawed in Arctic lakes since the 1950s, *Nature Geoscience*, 9, 679-682, 10.1038/ngeo2795, 2016.
- 725 Walter, K. M., Zimov, S., Chanton, J. P., Verbyla, D., and Chapin, F. S.: Methane bubbling from Siberian thaw lakes as a positive feedback to climate warming, *Nature*, 443, 71-75, 2006.
- Xie, Y., Sha, Z., and Yu, M.: Remote sensing imagery in vegetation mapping: a review, *Journal of Plant Ecology*, 1, 9-23, 10.1093/jpe/rtm005, 2008.
- 730 Zuidhoff, F. S. and Kolstrup, E.: Changes in palsa distribution in relation to climate change in Laivadalen, northern Sweden, especially 1960–1997, *Permafrost and Periglacial Processes*, 11, 55-69, [https://doi.org/10.1002/\(SICI\)1099-1530\(200001/03\)11:1<55::AID-PPP338>3.0.CO;2-T](https://doi.org/10.1002/(SICI)1099-1530(200001/03)11:1<55::AID-PPP338>3.0.CO;2-T), 2000.